

Early-Stage Formation of Helical Single Crystals and Their Confined Growth in Thin Film

Christopher Y. Li, Jason J. Ge, Feng Bai, Bret H. Calhoun, Frank W. Harris, and Stephen Z. D. Cheng*

The Maurice Morton Institute and Department of Polymer Science, The University of Akron, Akron, Ohio 44325-3909

Liang-Chy Chien

Liquid Crystal Institute, Kent State University, Kent, Ohio 44010-0001

Bernard Lotz

Institute Charles Sadron, 6 Rue Boussingault, Strasbourg 67083

H. Douglas Keith

Institute of Materials Science, University of Connecticut, Storrs, Connecticut 06269

Received December 27, 2000; Revised Manuscript Received March 23, 2001

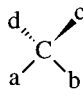



ABSTRACT: We have previously reported on flat (lathlike) and helical single crystals grown from a smectic A* liquid crystalline (LC) phase of a main-chain nonracemic chiral polymer, PET(R*-9), synthesized from (R)-(-)-4'-[ω -[2-(*p*-hydroxy-*o*-nitrophenyloxy)-1-propyloxy]-1-nonyloxy]-4-biphenylcarboxylic acid.^{1,2} In this paper, we focus on the formation and growth process of these two types of crystals on the surface of a carbon-coated glass substrate. This substrate provides confinement that affects the crystallization process and ultimately prohibits the development of helical crystals when the film thickness is less than a few tens of nanometers. The population of helical crystals increases as the film thickness increases. Furthermore, at the same crystallization temperature, the pitch lengths of these helical crystals vary in films with different thickness. Coexistence of flat and helical forms in the same lamellar crystal can also be found, suggesting the possibilities of sudden changes of chain packing between them. Early stages of the formation of the helical crystals have been studied using a solvent washing technique for partially crystallized droplets. Uncrystallized LC PET(R*-9) is dissolved while helical lamellae are exposed, and at an early stage of growth, these crystals are observed to be saddle-shaped. Primary nucleation initiates planar growth which develops into saddle-shaped crystals as growth proceeds along both long and short axes of these flat crystals. Crystal growth rates are such that molecular diffusion can occur over distances on the order of micrometers in the surrounding mobile LC phase during crystallization.

Introduction

Lord Kelvin's phenomenological definition of "chirality" is as follows: "I call any geometrical figure or group of points 'chiral', and say it has 'chirality', if its image in a plane mirror, ideally realized, cannot be brought into coincidence with itself."³ This concept does not impose size limitations. Generally speaking, four levels of chirality on different length scales may usefully be identified in polymers: the configurational, conformational, phase, and object chirality.⁴ Table 1 summarizes these four levels of chirality, their length scales, typical examples, and experimental methods used to study them. Configurational chirality at the atomic level is represented by molecular chiral centers, originating from different chemical groups covalently bonded to an atom. Conformational chirality is attributed to different handedness of helical conformations in molecules. The phase chirality is associated with helical phase structures such as twisted lamellar crystals and monodomains of chiral liquid crystalline (LC) phases. Aggregation of the chiral phase structures can result in a chiral macroscopic object, as in some banded spherulites, which completes the highest level of this chirality hierarchy.⁴

* To whom correspondence should be addressed. E-mail: cheng@polymer.uakron.edu.

Table 1. Four Levels of Chirality in Different Length Scales

Hierarchies	1 st Level Configuration	2 nd Level Conformation	3 rd Level Phase	4 th Level Object
Scale	0.1 - 1 nm	nm - μ m	50nm - 100 μ m	> 1 μ m
Schematic Representations				
Examples	Atom Sites	Polymer Chains	Helical Assembly, LC Monodomains	Aggregates of 3 rd Chiral Phase
Studying Methods	Polarimetry...	CD, X-ray...	Microscopy, X-ray, Light Scattering...	Microscopy, X-ray, Light Scattering...

Asymmetric synthesis deals with the configurational chirality, which has been rapidly developed over the past 30 years.^{5–7} Research on conformational chirality dates back several decades regarding DNA conformations.⁸ Most work has been focused on controlling the handedness of helical polymer chains by tuning their chemical residues and external factors such as pH values, solvents, temperature, light, and salt concentrations.^{9–11} Compared with the first two levels of chirality, the third level of chirality is less recognized in polymers although reports can be found as early as in the 1970s in larger length scale helical assembled morphologies.

Examples are the helical supercoil of PBLG strands,¹² helical single crystals of *B. Mori* silk,¹³ and the helical phases of chiral liquid crystals.^{14–17} On a macroscopic scale, the handedness of banded spherulites in chiral synthetic polymers also provides clear evidence for object chirality.^{18–20}

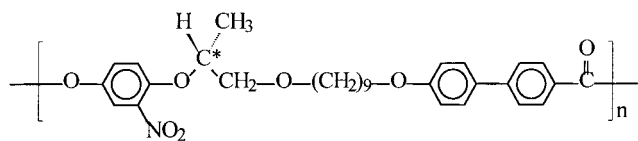
To understand interrelationship and interdependence between different levels of chirality in chiral polymers, packing schemes on different length scales have to be taken into account. It has been experimentally observed that chiral molecules with a helical conformation do not necessarily pack into a chiral assembly. On the other hand, some configurationally achiral molecules can possess a helical conformation and morphology. One example is the so-called bent-core liquid crystals whose helical phase morphology has been reported even though their chemical structures are achiral. It is the molecular bent shape instead of the chiral molecular centers that introduces symmetry breaking and leads to the helical morphology.^{21–23} Another example is polyethylene (PE), whose spherulites exhibit twisted (banded) texture resulting from a progressive rotation of molecular orientation.^{24–27}

Recently, we have designed a series of main-chain LC nonracemic chiral polyesters [PET(R*-*n*)] with a right-handed chiral center (R*) synthesized from (*R*)-(-)-4'-{ω-[2-(*p*-hydroxy-*o*-nitrophenyloxy)-1-propyloxy]-1-nonyloxy}-4-biphenylcarboxylic acid.²⁸ For samples having nine methylene units, PET(R*-9), under the same crystallization conditions both flat (lathlike) and helical single lamellar crystals were observed. Within the flat crystals, the apparent crystal structure is orthorhombic with unit cell dimensions $a = 1.07$ nm, $b = 0.48$ nm, and $c = 5.96$ nm.^{1,2} Helical crystals, on the other hand, show a superimposed twisting of chain orientation, implying a progressive deviation of unit cells and of chain orientations within nominally orthorhombic unit cells.^{4,29} The thickness of a single lamella is about 15–20 nm, depending upon crystallization temperatures (T_c). In most cases, multilamellar layers are found. The molecular chains are normal to the plane of the lamella, and the fold direction is aligned parallel to the long lamellar or helical axis (the *b*-axis).²

In this paper, we focus upon confinement effects of carbon-coated glass substrates on helical crystal growth and how flat and twisted crystal morphologies can both form under similar crystallization conditions and share so many structural similarities. We have monitored initial growth in helical crystals in order to explore the role of molecular diffusion in their formation.

Experimental Section

Materials and Sample Preparation. The chemical structure of PET(R*-9) is



The specific rotation of the monomers is $[\alpha]_D = -28.5^\circ$. The molecular weight of PET(R*-9) is around 16 000 g/mol, and the polydispersity is approximately 2 after fractionations, as measured by gel permeation chromatography based on polystyrene standards.

Polymer thin films (with a thickness of around 50–100 nm) were prepared via solution casting from a 0.05% (w/v) tetra-

hydrofuran (THF) solution. After the solvent was evaporated, the films were heated in a hot stage (Mettler FP-90) to above the highest endothermic transition temperature (190 °C) and were subsequently quenched to preset temperatures. The samples were held isothermally for various time periods ranging from several hours to a few days under conditions where crystallization occurred from a smectic A* phase. The samples were then quenched in liquid nitrogen and equilibrated at room temperature, which was below the glass transition temperature of this polymer ($T_g = 37$ °C). The thin-film samples prepared for transmission electron microscopy (TEM) observations were first examined under both polarized light microscopy and phase contrast microscopy before they were shadowed by Pt and coated with carbon for TEM observations. The shadowing process was not applied for the samples used in dark field (DF) experiments. Relatively thick films and droplets were also prepared using 0.1% (w/v) THF solution.

Equipment and Experiments. TEM experiments were carried out to examine crystal morphology in a JEOL (1200 EX II) TEM using an accelerating voltage of 120 kV. Selected area electron diffraction (ED) patterns of the samples having different zones were also obtained. Calibration of the ED spacings was done using TiCl in a d spacing range smaller than 0.384 nm, which is the largest spacing for TiCl. Spacing values larger than 0.384 nm were calibrated by doubling the d^* -spacing of those diffractions based on their first-order diffractions. DF images were obtained using specific (*hkl*) ED spots in order to determine the chain orientation in both of the flat-elongated and helical lamellar crystals.

Solvent washing experiments were conducted using THF in order to observe the early stages of crystal growth and morphological formation. The washing time is approximately 5–20 s depending upon the dimensions of the partially crystallized polymer droplets. It was expected that the washing process only dissolved away uncrystallized regions of the samples, and crystalline regions of the samples were retained. After washing, the underlying lamellar crystals were decorated using polyethylene (PE) oligomers as described in refs 30 and 31. This decoration method was also applied to the well-developed lamellar crystals.

Results and Discussion

Confinement Effects on the Flat and Helical Lamellar Crystals. Confinement effects are presumably important factors in governing the formation of crystals in films. A carbon-coated glass substrate provides a rigid adherent interface and for thin-film samples can generally be viewed as favoring the growth of flat crystals. However, observations of helical crystals growing in thicker films on the same kind of substrate indicate that substrate effects can be frustrated when growth is no longer tightly confined. We have prepared relatively thick film samples (thicknesses of ~ 1 μ m) in which the occurrence of helical crystals is indeed significantly higher ($\sim 80\%$) than in thinner films of ~ 50 nm thickness ($\sim 30\%$). Both types of morphology may also occasionally occur in the same crystal as shown by TEM micrographs in Figure 1, taken from a sample crystallized at 145 °C for 24 h. Boundaries between the two types of morphology vary in orientation, being nearly parallel to the short crystal axis (the *a*-axis) in Figure 1a, parallel to the long crystal axis (the *b*-axis) in Figure 1b, and oblique to the long axis as in Figure 1c (in this case by 20°). Figure 1d is a PE-decorated PET(R*-9) crystal having both flat and helical morphology. The helical part lies on top of the flat crystal and possibly originated from screw dislocations formed during crystal growth. PE oligomer crystal rods are perpendicular to the long axis on both parts of the crystal. The chain folding direction is thus identical in both parts of the crystal and is parallel to the *b*-axis.

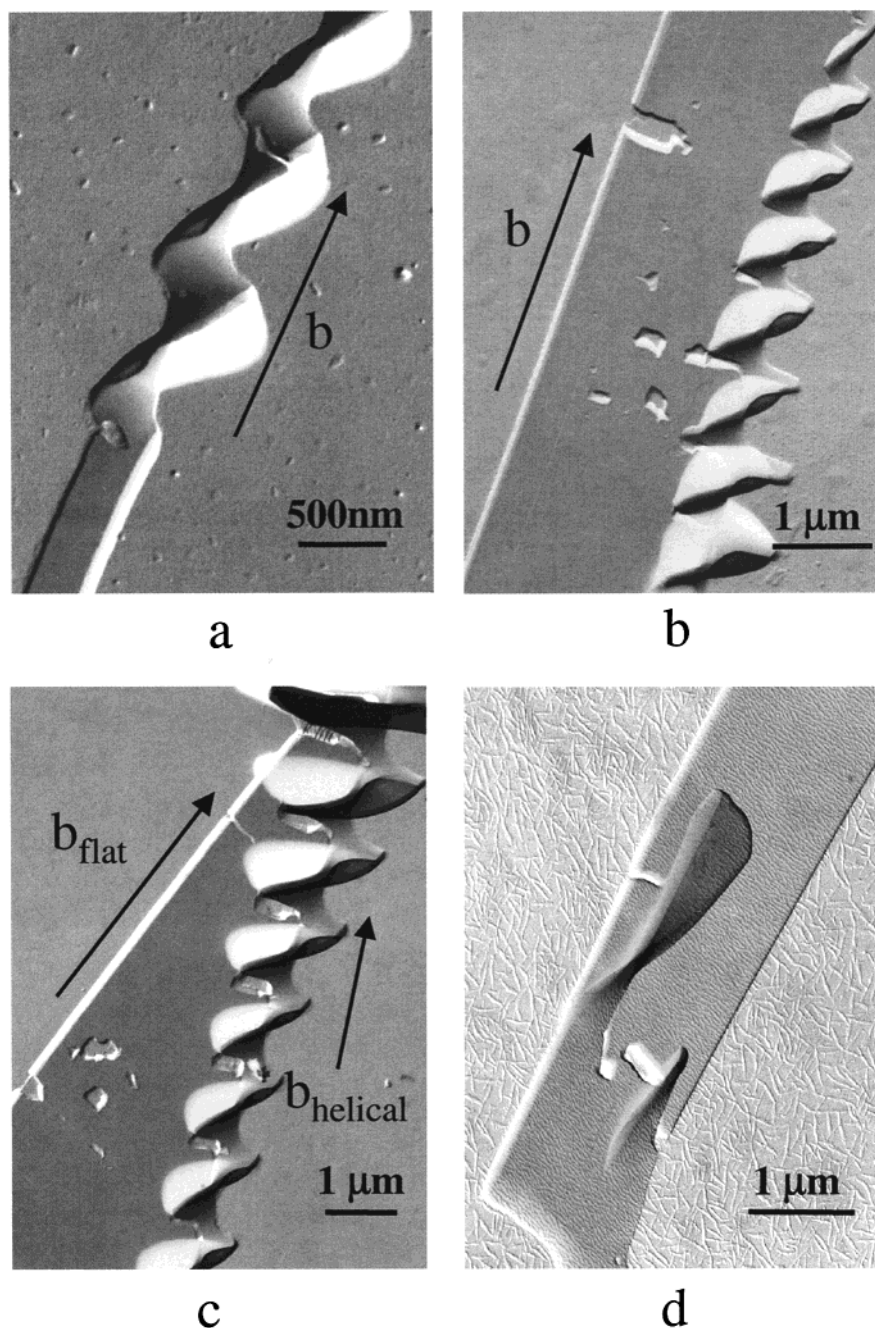


Figure 1. TEM micrographs of coexisting flat and helical crystals. The interface between the two could be nearly parallel to the short axis (the a -axis) (a), the long axis (the b -axis) (b), or even at an oblique angle (20° in this figure) with respect to the flat crystal long axis (c). Helical crystals can also be seen on top of a flat basal one, possibly originating from screw dislocations (d). PE decoration in (d) shows that there is no sudden change of the chain-folding behavior between these two types of crystals. All of these crystals were isothermally crystallized at 145°C for 24 h.

To examine the molecular orientation changes in both flat and helical parts of the crystal, DF experiments using the $(20l)$ diffraction spots of the crystals having both flat and helical parts were carried out, and the results are shown in Figure 2. In the flat part, a bright zone runs parallel to the crystal long axis (the b -axis), while bright lines are nearly perpendicular to this axis in the helical part. These results suggest that the polymer chains change their orientations between the flat and the helical parts at the boundary. In the flat part, chains are perpendicular to the b -axis. However, within each cross section of the crystal perpendicular to the b -axis, the chains are not exactly parallel to each other but rather they are slightly splayed (as evidenced by the bright zone, instead of an entire bright area in

the DF results).⁴ Also, molecular chains twist about the short axis (the a -axis) in addition to twisting about the long helical axis in the helical part.^{4,30}

Crystals Developed on Solid Substrate in the Early Stage of Growth. Figure 3 shows a fully developed helical crystal as revealed by TEM. The helix is wider in the upper part (A) of the crystal and narrower in the bottom part (B) of the crystal. The pitch length also gradually changes from 3.0 to $5.8\ \mu\text{m}$. Since formation of the helical morphology depends on many factors such as nucleation density, film thickness, availability of material, etc., it is difficult to explain the evolution of this crystal by having only the final morphology to go on. The ideal would be to observe the crystals at consecutive early stages of crystal growth.

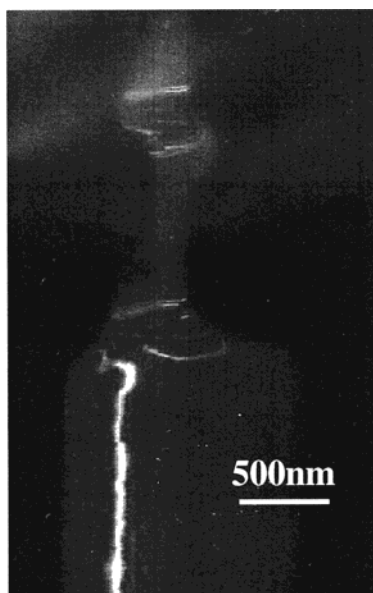


Figure 2. A (20) TEM DF micrograph of a crystal having coexisting flat and helical parts. The bright lines indicate the areas which give diffraction. The bright line is parallel to the crystal long axis on the flat part and perpendicular to the crystal long axis on the helical part, indicating different chain orientations in these two types of crystals.

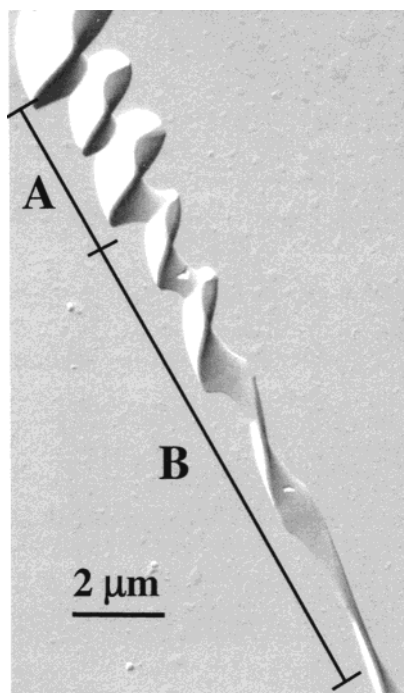


Figure 3. TEM micrograph of a fully developed helical single crystal. The upper part (A) of the crystal is wider than the bottom part (B) and has smaller pitch length. It is assumed that the upper part A was formed earlier in a droplet with more available material while the lower part B of the crystal was formed during the later stage of crystal growth (see text).

For this reason, we purposely prepared relatively thick droplets with diameters of approximately 0.5–3 μm . The center of the droplets is around 1–2 μm thick. Figure 4 shows crystals formed in four droplets after they were crystallized for 4 h at 145 $^{\circ}\text{C}$ (note that the micrograph is a negative). The bright bands within the droplets represent the crystal parts which may deviate from the flat-on arrangement and be the early stages of the helical crystals (one of them is pointed out by an

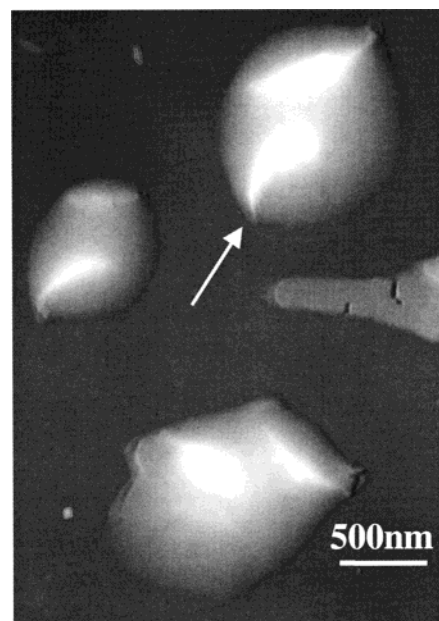


Figure 4. TEM micrograph (negative film) of dewetted droplets crystallized at 145 $^{\circ}\text{C}$ for 4 h. There are four droplets in this figure. Three of them have more or less retained their original shapes, and the fourth one in the middle-right side of the figure (which is only partially shown in the figure) started to develop a flat lamella outside of the droplet. The bright bands within the other droplets possibly indicate parts of crystals which have begun to deviate from the flat-on arrangement to form helical crystals (see Figure 6).

arrow in the figure), whose visibility is a result of mass contrast. However, in Figure 4 the crystals cannot be directly seen since they are embedded in the uncrystallized PET(R*-9) which is in the LC smectic A* phase.³² It can also be seen in the same figure that a flat lamellar crystal has formed and developed beyond the original boundary of the middle right-side droplet.

After THF washing of the partially crystallized droplets to remove uncrystallized polymer, the crystalline parts within the droplets could be seen. Figure 5 shows the resulting morphology. In Figure 5a, a remaining helical crystal can be observed. The bright bands in Figure 4 would correspond to the upper edge-on part of the helical crystal in Figure 5a, which indeed starts to deviate from the flat-on part at the center of the crystal. On the lower left-hand side of Figure 5a, a flat crystal can be seen which formed between two neighboring droplets (the lower droplet is not shown in the figure) in originally thinner film, where the substrate confinement is more effective favoring the formation of flat crystals. Also note that only approximately 20% of the crystals formed in the droplets are flat. Figure 5b is such an example. This is possibly due to flat-on primary nucleation at/or very near surface of the substrate.

In Figure 5a, the helical crystal width is uniform well within the droplet. As the growth front advances toward the edges of the droplet, however, the growth environment gradually changes: the droplet thickness decreases outwardly, and the surface tension, which provides an additional anchoring energy for molecules to overcome, starts to play a role in the crystal growth. Figure 6 (the sample was crystallized for 4 h, washed with THF, and then decorated with PE) shows that, near the center of the droplet where the primary nucleation was initiated with a flat-on arrangement, the crystal width is wider (1.88 μm). When it gradually grew

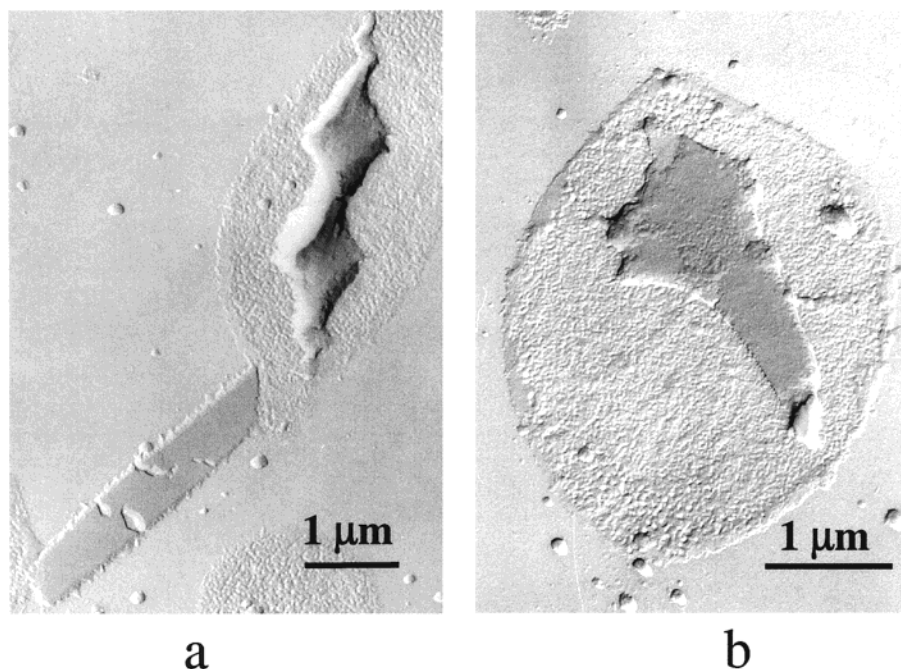


Figure 5. TEM micrographs of partially crystallized droplets after being washed with THF show a helical lamellar crystal (a) and a flat lamellar crystal (b).

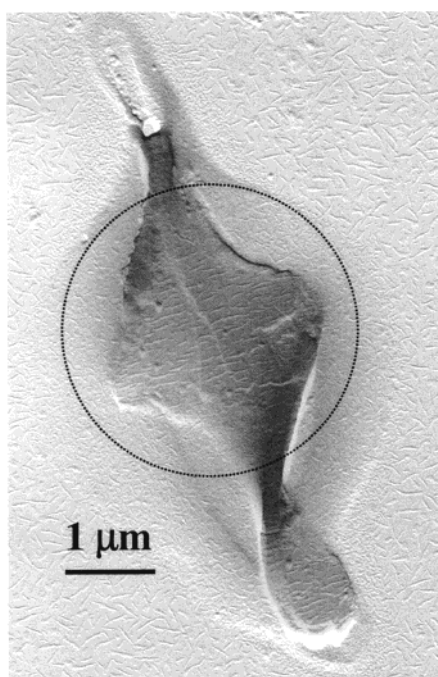


Figure 6. TEM micrograph of a partially crystallized droplet after being washed with THF and decorated with PE. This confirms that the bright bands in Figure 4 correspond to crystal edges which start to deviate from the flat-on part. The initial part (dotted circle) of the crystals resemble a "saddle plane" with one of its diagonal directions parallel to the helical axis.

to form a helical crystal toward the edges of the droplet, the crystal turns over by 180°. The tips of the helical crystal growth become narrower (0.68 μm). It is presumable that the wider crystal area exercises larger stresses to detach from the substrate. The narrower tips may be caused by the thin edge of the droplet and depletion of polymers.

The crystal within the dotted circle is saddle-shaped, representing the early stage growth of the helical crystal

within the droplet. It is not surprising, purely as a matter of geometry, if lamellar twist is inevitably a second twist of opposite hand about an axis transverse to that of the main (helical) twist. Between these two twists, therefore, there must be saddle geometry. This is an expected natural growth habit when unconstrained growth is an elongated twisted helical lamella. Furthermore, PE crystalline rods on the saddle-plane surface are perpendicular to the long helical axis, indicating that the chain-folding direction is along the long axis (the *b*-axis) of the crystal.¹ This suggests that the chain-folding direction has been already established at this early stage of the crystallization.

It is also interesting that in Figure 3 the pitch length of the helical single crystal changes. In the case of chiral liquid crystals, such as in the cholesteric phase, their pitch length is usually temperature and/or concentration dependent.³³ For PET(R*-9) helical crystals in the thermotropic form, the helical single-crystal morphology exhibits different pitch lengths even at a constant T_c . Figure 7 further provides two examples of stacks of helical lamellar crystal morphologies with similar thickness of ~ 100 nm (stacks of multiple lamellae) but different pitch lengths formed at $T_c = 145$ °C, which range from 0.8 μm (Figure 7a) to 6 μm (Figure 7b). For helical crystals with pitch lengths of 0.8 and 6 μm , therefore, the tilting angles of each layer along the *b*-axis can be calculated, based on the molecular chain packing in the crystal unit cell ($b = 0.48$ nm), and they are 0.21° and 0.03°, respectively.

Molecular Diffusion in Developing Helical Single Crystals under Confinement. A remaining question is as to how the molecular chains diffuse on a two-dimensional surface during the crystallization in a thin film on a substrate. This is more critical in the case of single crystal growth from droplets. Within the droplet, polymer is readily available, while out of the droplet some of the polymer will have to migrate from the droplet to the growth fronts. Figure 8 shows helical crystals grown from a droplet of PET(R*-9) after isothermal crystallization at 150 °C for 24 h. The dotted

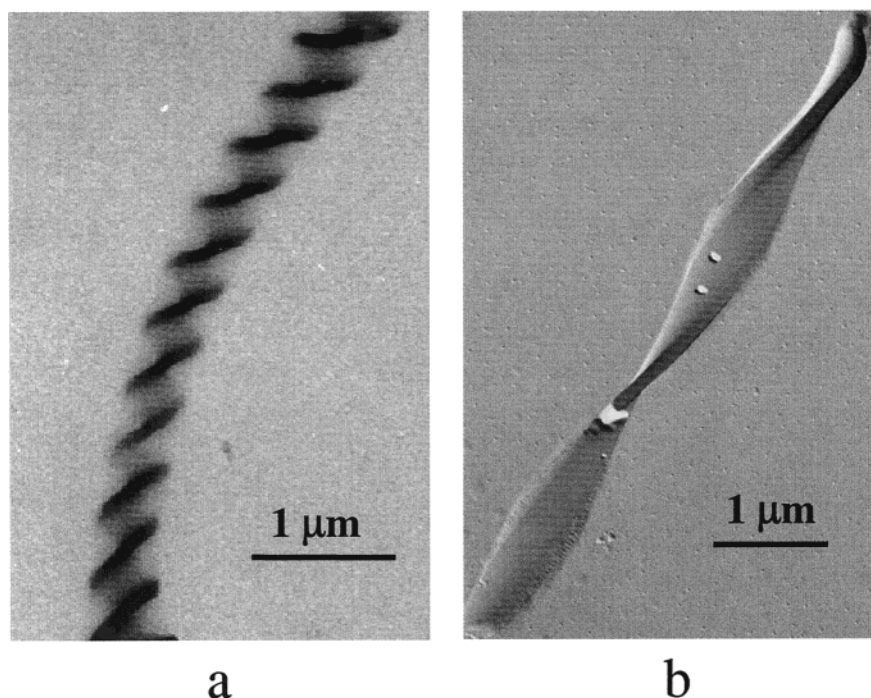


Figure 7. TEM micrographs of two helical crystals grown in the same crystallization condition of 145 °C for 24 h: (a) the pitch length is 0.8 μm , and (b) the pitch length is 6 μm .

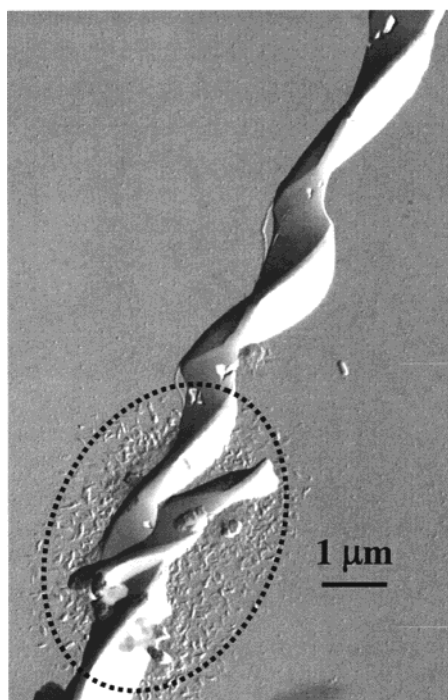


Figure 8. TEM micrograph of helical lamellar crystals, which started to grow in a droplet (a dotted circle). The isothermal crystallization was carried out at 150 °C for 24 h.

circle in this figure is the initial droplet area, and the helical crystal was grown from this circular area. The continuous growth of the helical crystal requires a large-scale molecular diffusion. An interesting feature is that there are two helical crystals grown in the droplet, and one is on the top of the other. The helical crystal on the top did not develop further due presumably to the lack of material and the thickness confinement of the droplet. Indeed, there may be a multiple number of helical crystals grown within one droplet as shown in Figure 9 (six infant helical crystals) in which the sample was



Figure 9. TEM micrograph of multiple (six) infant helical crystals developed within one droplet as seen after THF washing. The isothermal crystallization was carried out at 150 °C for 4 h.

crystallized at 150 °C for 4 h followed by THF washing. All of the helical crystals are constrained within the droplet. Figure 9 may actually also represent an initial stage of developing the helical crystal packing in the bulk state.

It has to be noted that, in order to form helical crystals, molecules need to migrate not only along the substrate surface but also away from this surface. For example, a helical crystal having a width of 1 μm requires molecules to migrate 1 μm upward above the substrate surface when the lamella is twisted to the edge-on arrangement. The main driving force of this diffusion must be the crystallization process having slow

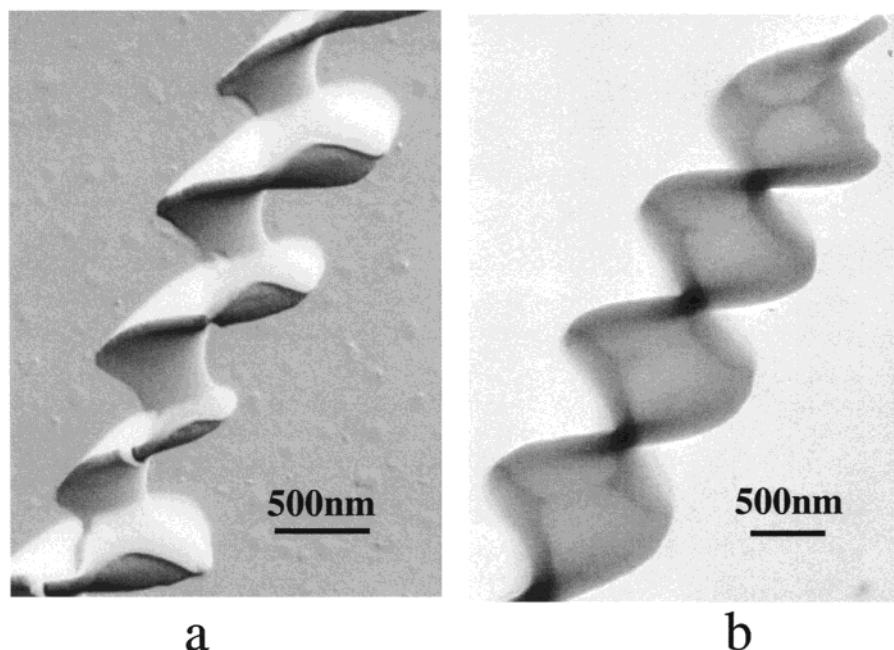


Figure 10. Two TEM micrographs of helical crystals: (a) asymmetric helical crystal and (b) symmetric helical crystal after isothermal crystallization at 150 °C for 24 h (see text).

growth rates. Further investigation is necessary to understand this molecular diffusion process during the crystallization.

The geometric confinement of the substrate can also be identified by an asymmetric shape in the helical crystals grown from thin films as shown in Figure 10a. The upper helical part of the crystal above the central long helical axis in this figure is wider than the lower part under this helical axis. This may be due to the fact that the gap distance between the long helical axis and the substrate is small during the crystal growth. The growth of the lower part is constrained by the hard substrate surface while there is less space restriction for the growth of the upper part. Therefore, as long as enough material and sufficient migration of molecules can reach the upper part of the helical crystal, overgrowth along the width direction on the upper part breaks the screw-axis symmetry of the helical crystal. For comparison, Figure 10b shows a symmetric helical crystal. The long helical axis in this case is approximately located at the center of the helical crystal, and the upper and lower parts of the crystal grow with screw-axis symmetry along this helical axis.

Conclusions

In summary, confinement by the solid substrate has a major effect on the PET(R*-9) flat and helical crystal growth from thin films. The substrate provides a flat geometry, and therefore, the thinner film sample prefers to grow flat single crystals while the thicker film aids in the formation of the helical crystals. Coexistence of the flat and helical parts in one crystal has also been observed. The transformation between these two parts is associated with different molecular orientations which generate large grain boundaries. Helical crystals having different pitch lengths have been found, even though they are crystallized at an identical T_c . The tilting angles between adjacent molecular layers along the long helical axis (the b -axis) thus vary in these helical crystals having different pitch lengths. Using polymer droplets and the solvent-washing technique, early stages

of the helical crystal growth can be observed. They are typified by the formation of a "saddle-shaped" lamella followed by twisted growth along two tips to form the long helical axis. It is evident that large-scale molecular diffusion and migration happen during the slow crystal growth. Asymmetric helical crystals have been frequently observed due to the overgrowth of the upper part of the helix and the confinement of the substrate which limits the growth of the lower part of the helical crystals.

Acknowledgment. We are grateful for the funding from NSF (DMR-9617030) and NSF ALCOM Science and Technology Center (DMR-8920147). Thoughtful and in-depth discussions with Dr. F. Khoury at NIST regarding this topic are greatly acknowledged.

References and Notes

- (1) Li, C. Y.; Yan, D.; Cheng, S. Z. D.; Bai, F.; Ge, J. J.; He, T.; Chien, L. C.; Harris, F. W.; Lotz, B. *Phys. Rev. B* **1999**, *60*, 12675.
- (2) Li, C. Y.; Yan, D.; Cheng, S. Z. D.; Bai, F.; Ge, J. J.; He, T.; Chien, L. C.; Harris, F. W.; Lotz, B. *Macromolecules* **1999**, *32*, 524.
- (3) Thomson, W. *The Robert Boyle Lecture*, Oxford University Junior Scientific Club, May, 1883, in Baltimore Lectures (London: C. J. Clay & Sons), 1904.
- (4) Li, C. Y.; Cheng, S. Z. D.; Ge, J. J.; Bai, F.; Zhang, J. Z.; Mann, I. K.; Chien, L. C.; Harris, F. W.; Lotz, B. *J. Am. Chem. Soc.* **2000**, *122*, 72.
- (5) Okamoto, Y.; Nakano, T. *Chem. Rev.* **1994**, *94*, 349.
- (6) Special issue on Enantioselective Synthesis: *Chem. Rev.* **1992**, *94*, 739.
- (7) Rowan, A. E.; Nolte, R. J. M. *Angew. Chem., Int. Ed. Engl.* **1998**, *37*, 63.
- (8) Saenger, W. *Principles of Nucleic Acid Structure*; Springer-Verlag: New York, 1984.
- (9) Blout, E. R.; Carver, J. P.; Gross, J. *J. Am. Chem. Soc.* **1963**, *85*, 644.
- (10) Matsumoto, M.; Watanabe, H.; Yoshioka, K. *Biopolymers* **1973**, *12*, 1729.
- (11) Yashima, E.; Maeda, Y.; Okamoto, Y. *J. Am. Chem. Soc.* **1998**, *120*, 8895.
- (12) Rybníkar, F.; Geil, P. H. *Biopolymers* **1972**, *11*, 271.
- (13) Lotz, B.; Gonthier-Vassal, A.; Brack, A.; Magoshi, J. *J. Mol. Biol.* **1982**, *156*, 345.

- (14) Saupe, A. *Angew. Chem., Int. Ed. Engl.* **1968**, *7*, 97.
- (15) Helfrich, W.; Oh, C. S. *Mol. Cryst. Liq. Cryst.* **1971**, *14*, 289.
- (16) Goodby, J. W.; Waugh, M. A.; Stein, S. M.; Chin, E.; Pindak, R.; Patel, J. S. *Nature* **1989**, *337*, 449.
- (17) Goodby, J. W.; Slaney, A. J.; Booth, C. J.; Nishiyama, I.; Vuijk, J. D.; Styring, P.; Toyne, K. J. *Mol. Cryst. Liq. Cryst.* **1994**, *243*, 231.
- (18) Singfield, K. L.; Hobbs, J. K.; Keller, A. *J. Cryst. Growth* **1998**, *183*, 683.
- (19) Saracovan, I.; Cox, J. K.; Revol, J.-F.; Manley, R. St. J.; Brown, G. R. *Macromolecules* **1999**, *32*, 717.
- (20) Saracovan, I.; Keith, H. D.; Manley, R. S. J.; Brown, G. R. *Macromolecules* **1999**, *32*, 8918.
- (21) Niori, T.; Sekine, T.; Watanabe, J.; Furukawa, T.; Takezoe, H. *J. Mater. Chem.* **1996**, *6*, 1231.
- (22) Link, D. R.; Natale, G.; Shao, R.; MacLennan, J. E.; Clark, N. A.; Krblova, E.; Walba, D. M. *Science* **1997**, *278*, 1924.
- (23) Heppke, G.; Moro, D. *Science* **1998**, *279*, 1872.
- (24) Keith, H. D.; Padden, F. J., Jr. *J. Polym. Sci.* **1959**, *39*, 101.
- (25) Keller, A. *J. Polym. Sci.* **1959**, *39*, 151.
- (26) Keith, H. D.; Padden, F. J., Jr. *Polymer* **1984**, *25*, 28.
- (27) Keith, H. D.; Padden, F. J., Jr. *Macromolecules* **1996**, *29*, 7776.
- (28) Bai, F.; Chien, L. C.; Li, C. Y.; Cheng, S. Z. D.; Percheck, R. *Chem. Mater.* **1999**, *11*, 1666.
- (29) Li, C. Y.; Cheng, S. Z. D.; Ge, J. J.; Bai, F.; Zhang, J. Z.; Mann, I. K.; Chien, L.-C.; Harris, F. W.; Yan, D.; He, T.; Lotz, B. *Phys. Rev. Lett.* **1999**, *83*, 4558.
- (30) Wittmann, J. C.; Lotz, B. *Makromol. Rapid Commun.* **1982**, *3*, 733.
- (31) Wittmann, J. C.; Lotz, B. *J. Polym. Sci., Polym. Phys. Ed.* **1985**, *23*, 205.
- (32) Li, C. Y.; Ge, J. J.; Bai, F.; Zhang, J. Z.; Calhoun, B. H.; Chien, L. C.; Harris, F. W.; Cheng, S. Z. D. *Polymer*, **2000**, *41*, 8953.
- (33) Buckingham, A. D.; Ceasar, G. P.; Dunn, M. B. *Chem. Phys. Lett.* **1969**, *3*, 540.

MA0021996